

# Infrared phonon activity in pristine graphite

M. Manzardo <sup>\*,1</sup> E. Cappelluti,<sup>2,3</sup> E. van Heumen <sup>†,4</sup> and A.B. Kuzmenko<sup>4</sup>

<sup>1</sup>*Dipartimento di Fisica, "Sapienza" Università di Roma, P.le A. Moro 2, 00185 Roma, Italy*

<sup>2</sup>*Instituto de Ciencia de Materiales de Madrid, CSIC, 28049 Cantoblanco, Madrid, Spain*

<sup>3</sup>*ISC-CNR, via dei Taurini 19, 00185 Roma, Italy*

<sup>4</sup>*DPMC, Université de Genève, 1211 Genève, Switzerland*

(Dated: November 8, 2018)

We study experimentally and theoretically the Fano-shaped phonon peak at  $1590\text{ cm}^{-1}$  ( $0.2\text{ eV}$ ) in the in-plane optical conductivity of pristine graphite. We show that the anomalously large spectral weight and the Fano asymmetry of the peak can be qualitatively accounted for by a charged-phonon theory. A crucial role in this context is played by the particle-hole asymmetry of the electronic  $\pi$ -bands.

The discovery of graphene has triggered a tremendous amount of activity to study the electronic and structural properties of single-layer and multi-layer graphitic compounds. The presence, in optical probes, of phonon anomalies related to the in-plane carbon displacements has in particular been useful both for the characterization and for the investigation of the fundamental properties of graphene. While initially Raman spectroscopy was mainly employed,<sup>1–7</sup> recent infrared experiments in bilayer and multilayer graphene have significantly contributed to the field, showing new remarkable phenomena, such as a strong modulation of the magnitude and of the lineshape of the optical phonon peaks as function of electrostatic gating,<sup>8,9</sup> the number of layers,<sup>10</sup> and chemical doping.<sup>11</sup>

The interest to graphene has also given a new impulse to the research on its 3D parent material, graphite. One of the long standing problems is the origin in graphite of the infrared phonon activity in the optical conductivity at  $\omega \approx 0.2\text{ eV}$ , which is associated with the in-plane  $E_u$  carbon displacements. Early measurements of the peak intensity, expressed in terms of the effective infrared charge  $Z$ , range from  $Z = 0.18$  to  $Z = 0.41$  electrons per atoms,<sup>12,13</sup> qualitatively confirmed by more recent measurements.<sup>14,15</sup> The possible origin of the infrared activity of the  $E_u$  mode in pristine graphite was theoretically investigated in Ref. 16 by means of a generalized bond-charge model. The predicted phonon intensity was however significantly smaller than the experimental results.

In this work we combine experiment and theory in order to gain new insights into this problem. Our infrared measurements on highly ordered pyrolytic graphite (HOPG)<sup>18</sup> allowed us to characterize both the intensity and the Fano asymmetry of the phonon anomaly. We analyze these results within the context of the charged-

phonon theory,<sup>20</sup> which has recently been shown to account quantitatively for the phonon infrared intensity in few-layer graphenes.<sup>10,17</sup> While in gated graphene the main factors that determine the infrared intensity are the induced doping and the internal electric field, here we show that in charge neutral graphite the phonon infrared activity is essentially driven by the tight-binding terms breaking the particle-hole symmetry.

Infrared reflectivity spectra were measured from 20 to  $6400\text{ cm}^{-1}$  at different temperatures from 10 K to 300 K, using Fourier transform spectroscopy and *in-situ* gold coating as a reference. The spectra are shown in Fig. 1. The inset expands the region around  $1600\text{ cm}^{-1}$ , where the phonon peak is located. Optical conductivity  $\sigma(\omega)$  was extracted by the Kramers-Kronig analysis, supported by spectroscopic ellipsometry between 6400 and  $36000\text{ cm}^{-1}$  as described in Ref. 18. The spectral resolution was  $5\text{ cm}^{-1}$ . Fig. 2a shows the real part of  $\sigma(\omega)$  near the phonon peak, where a smooth baseline due to direct electronic interband transitions was subtracted.

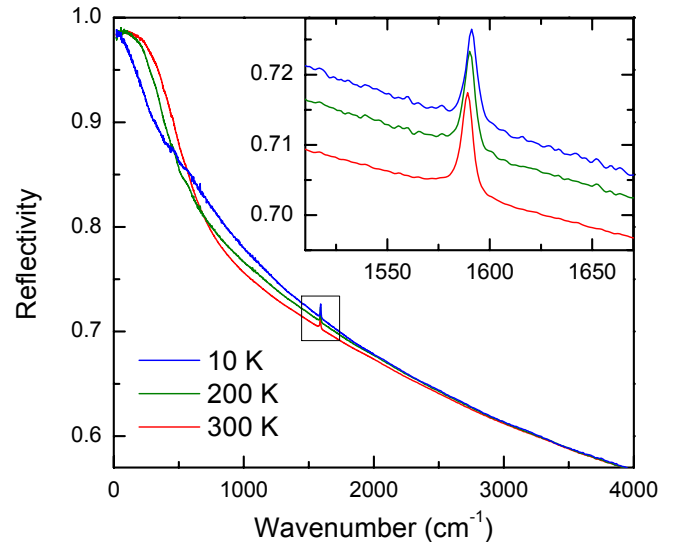


FIG. 1: Infrared reflectivity spectra of highly ordered epitaxial graphene at 300 K, 200 K and 10 K from Ref.18. The inset shows the region near the phonon peak.

\*Present address: Leibniz-Institut für Festkörperphysik und Werkstofforschung, Helmholtzstraße 20, Dresden, Germany

†Present address: van der Waals - Zeeman Institute, University of Amsterdam, Sciencepark 904, 1098 XH Amsterdam, the Netherlands

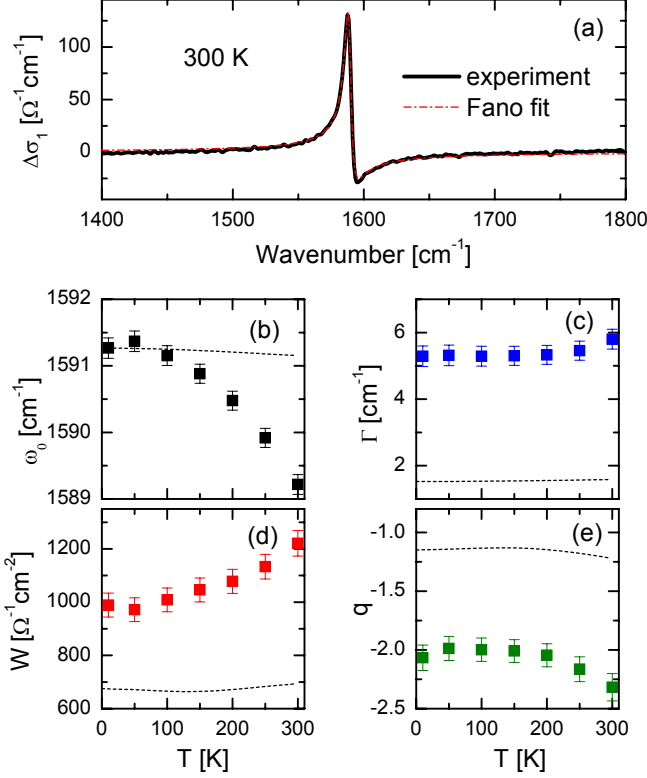


FIG. 2: (a) Real part of the optical conductivity  $\Delta\sigma_1(\omega)$  (thick black line) in the vicinity of the  $E_u$  phonon peak after a smooth background is subtracted. Also shown is the fitting curve (red line) as obtained by Eq. (1). Panels (b)-(e) show the phonon parameters  $\omega_0$ ,  $\Gamma$ ,  $W$ ,  $q$  extracted by the fit as a function of temperature (symbols) along with the theoretical calculations (dashed lines) not taking the phonon anharmonicity into account.

The most striking feature is a pronounced peak asymmetry, signaling a Fano interference.<sup>8–10,19</sup> Accordingly, the spectra at every temperature are fitted very well with a standard Fano formula:<sup>8,19</sup>

$$\Delta\sigma'(\omega) = \frac{2W}{\pi\Gamma} \frac{q^2 + 2qz - 1}{q^2(1 + z^2)}, \quad (1)$$

where  $z = 2(\omega - \omega_0)/\Gamma$ , and where  $\omega_0$  and  $\Gamma$  characterize the frequency and the linewidth of the phonon anomaly, while  $W$  and  $q$  represent the phonon spectral weight and the Fano asymmetry parameter, respectively. The temperature dependence of such phonon properties as extracted from the fit procedure is shown in Fig. 2(b)-(e). The phonon frequency decreases by about  $2 \text{ cm}^{-1}$  as the temperature increases from 10 K to 300 K. The spectral weight  $W$  increases from  $950 \text{ } \Omega^{-1}\text{cm}^{-2}$ , which corresponds to the variation of the infrared effective charge  $e^* = Ze$  from 0.28 to 0.31  $e$ , in a good agreement with the previous experiments.<sup>12,13,15</sup> The measured linewidth is close to  $5 \text{ cm}^{-1}$ , which means that it is probably determined by the spectral resolution used and exceeds the actual value.

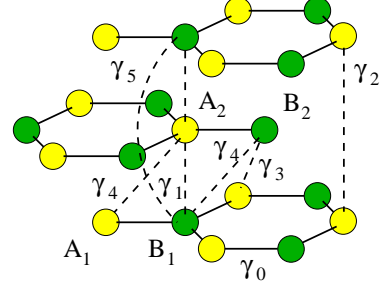


FIG. 3: (color online) (a) Atomic structure of graphite showing the relevant hopping terms  $\gamma_i$ . Atoms B1 and A2, connected by vertical  $\gamma_1$ , denoted by darker colors, contain also a local crystal field potential.

The observation of a finite infrared phonon intensity in pristine undoped graphite is quite intriguing given that it is a monoatomic compound. No infrared intensity would be expected for instance if all the carbon atoms were equivalent. Moreover the evaluation of the static dipole in realistic graphite through a tight-binding calculation finds, like in bilayer graphene, a charge-disproportion between the inequivalent sites (and hence a static electric dipole) three order of magnitude smaller than what observed.<sup>8</sup> A suitable framework to account for the finite infrared activity is thus the charged-phonon theory, which describes the borrowing of electronic effective charge by the optical mode from the electronic transitions to which it becomes coupled.<sup>20</sup> Such a theory has been successfully applied to bilayer graphene to explain the strong dependence of the phonon intensity and Fano asymmetry as functions of gating.<sup>17</sup>

A key role in this context is played by the mixed response function  $\chi(\omega)$ ,<sup>17</sup> which couples the current operator with the electron-phonon scattering operator related with the  $E_u$  lattice mode. The spectral weight is given by the relation  $W = \pi[\text{Re}\chi(\omega_0)]^2/\omega_0$ , while the asymmetry parameter is given by  $q = -\text{Re}\chi(\omega_0)/\text{Im}\chi(\omega_0)$ .

The analysis in Ref. 17 was performed within a simple tight-binding (TB) model, where only the nearest-neighbor in-plane and inter-plane hopping terms,  $\gamma_0$  and  $\gamma_1$ , were considered (see Fig. 3). Such model can be generalized in a straightforward way for the bulk graphite by introducing the interplane dispersion, so that  $\chi(\omega) \rightarrow \chi^{3D}(\omega) = \int_{-\pi}^{\pi} (dk_z/2\pi) \chi(k_z, \omega)$ , where  $\chi(k_z, \omega)$  is the mixed response function for bilayer graphene with the replacement  $\gamma_1 \rightarrow \gamma_1(k_z) = 2\gamma_1 \cos(k_z/2)$ . Note however that the description of the electronic structure of graphite in terms of this simple model would predict no infrared activity since the mixed response function would be zero. As we will show, the inclusion of high-order tight-binding terms, especially the ones that break the particle-hole symmetry, is fundamental to understand the origin of the phonon activity.

In order to perform a quantitative analysis we consider the full tight-binding model defined in the  $4 \times 4$  basis of the atomic orbitals  $\Psi_{\mathbf{k}}^\dagger = (a_{1\mathbf{k}}^\dagger, b_{1\mathbf{k}}^\dagger, a_{2\mathbf{k}}^\dagger, b_{2\mathbf{k}}^\dagger)$  where  $a_{i\mathbf{k}}^\dagger$

and  $b_{i\mathbf{k}}^\dagger$  represent the creation operators relative to the A and B sublattices in the layer  $i$ . The atomic basis and the different terms of the TB structure are shown in Fig. 3. The low energy bands of graphite around the K-H corner of the Brillouin zone are described by the Hamiltonian

$$\hat{H}_{\mathbf{k}} = \begin{pmatrix} \tilde{\gamma}_2 & v\pi^- & \tilde{v}_4\pi^- & \tilde{v}_3\pi^+ \\ v\pi^+ & \tilde{\gamma}_5 + \Delta & \tilde{\gamma}_1 & \tilde{v}_4\pi^- \\ \tilde{v}_4\pi^+ & \tilde{\gamma}_1 & \tilde{\gamma}_5 + \Delta & v\pi^- \\ \tilde{v}_3\pi^- & \tilde{v}_4\pi^+ & v\pi^+ & \tilde{\gamma}_2 \end{pmatrix}, \quad (2)$$

where  $\pi^\pm = \hbar(k_x \pm ik_y)$ ,  $\tilde{\gamma}_{1,3,4} = 2\gamma_{1,3,4} \cos(k_z d/2)$ ,  $\tilde{\gamma}_{2,5} = 2\gamma_2 + 2\gamma_{2,5} \cos(k_z d)$ ,  $\tilde{v}_{3,4} = v\tilde{\gamma}_{3,4}/\gamma_0$ . The paramagnetic current along the  $y$ -axis is thus evaluated as  $j_y = \sum_{\mathbf{k}, \sigma} \Psi_{\mathbf{k}}^\dagger \hat{j}_{\mathbf{k}y} \Psi_{\mathbf{k}}$  where  $\hat{j}_{\mathbf{k}y} = -(e/\hbar) \partial \hat{H}_{\mathbf{k}} / \partial k_y$ . The coupled electron-phonon interaction operator can be written as  $V = g \sum_{\mathbf{k}, \sigma} \Psi_{\mathbf{k}}^\dagger \hat{V}_{\mathbf{k}} \Psi_{\mathbf{k}} \phi_y$  where  $g$  is the electron-phonon coupling constant as defined in Ref. 17,  $\phi_y$  represents the dimensionless in-plane lattice displacement along the  $y$  direction. The precise form of  $\hat{V}$  depends on the TB model considered. In a simple model, where only  $\gamma_0$  and  $\gamma_1$  are present,  $\hat{V}_{\mathbf{k}}$  in graphite has the same expression as derived in Ref. 21 for bilayer graphene. In a full TB model, however,  $\hat{V}_{\mathbf{k}}$  requires the knowledge of the derivative of  $\gamma_4$  with respect to the lattice distortion  $u$ , in addition to the well known term  $d\gamma_0/du$ . The matrix  $\hat{V}_{\mathbf{k}}$  thus reads

$$\hat{V}_{\mathbf{k}} = \begin{pmatrix} 0 & 1 & -\alpha_4/\alpha_0\Gamma & 0 \\ 1 & 0 & 0 & \alpha_4/\alpha_0\Gamma \\ -\alpha_4/\alpha_0\Gamma & 0 & 0 & -1 \\ 0 & \alpha_4/\alpha_0\Gamma & -1 & 0 \end{pmatrix}, \quad (3)$$

where  $\Gamma = \cos(k_z d/2)$ . The deformation potentials  $\alpha_0 = d\gamma_0/du = 4.4 \text{ eV/\AA}$ ,  $\alpha_4 = d\gamma_4/du = 0.3 \text{ eV/\AA}$  are extracted from LDA calculations.<sup>22-24</sup>

Once the current  $j_y$  and the electron-phonon scattering operator  $V$  are defined, the phonon spectral properties can be evaluated in the framework of the charged-phonon theory following the derivation for bilayer graphene.<sup>17</sup> We evaluate the mixed response function in the bare-bubble approximation, where we obtain the analytical expression:

$$\chi(k_z, \omega) = \beta \sum_{\mathbf{k}, n, m} C_{y, \mathbf{k}}^{nm} \frac{f(\epsilon_{n, \mathbf{k}}) - f(\epsilon_{m, \mathbf{k}})}{\epsilon_{n, \mathbf{k}} - \epsilon_{m, \mathbf{k}} + \hbar\omega + i\eta}, \quad (4)$$

where  $n, m$  are band indices,  $C_{y, \mathbf{k}}^{nm} = (\hat{j}_{\mathbf{k}y})^{nm} (\hat{V}_{\mathbf{k}})^{mn}$  and  $f(\epsilon)$  is the Fermi function. We introduced a phenomenological damping term  $\eta$  to account for disorder effects. Finally,  $\beta = -igN_vN_s$ , where  $N_v = 2$  and  $N_s = 2$  stand for the valley and spin degeneracy, respectively.

In contrast to the case of the simple  $\gamma_0$ - $\gamma_1$  model, the inclusion of the higher-order TB terms makes  $\chi(\omega)$  dependent on the ultraviolet cutoff related to the finite bandwidth. To this aim we introduce in the linearized model a momentum cutoff  $k \leq \bar{k}$ , where  $\bar{k}$  is determined by requiring the conservation of the Brillouin zone,

TB model	p-h symmetry	$W$	$q$
full	broken	666	-1.15
partial: $\gamma_2$	broken	16	-0.53
partial: $\gamma_3$	preserved	-	-
partial: $\gamma_4$	broken	471	-0.94
partial: $\gamma_5$	broken	50	-0.47
partial: $\Delta$	broken	332	-0.74

TABLE I: The spectral weight  $W$  and the asymmetry parameter  $q$  at  $T = 0$  for the full TB model and for the partial TB models described in the text.  $W$  is expressed in units of  $\Omega^{-1} \text{ cm}^{-2}$ .

namely  $S_{\text{cell}} = \pi N_K \bar{k}^2$ . We get thus  $\bar{k} = 1.095 \text{ \AA}^{-1}$ , which is comparable with the distance  $\Gamma$ -K  $\approx 0.98 \text{ \AA}^{-1}$  of the hexagonal Brillouin zone.

To elucidate the role of the various TB parameters on the infrared phonon peaks, we consider for the moment the full set of TB parameters from Ref. 25. The phonon spectral properties obtained for this model retaining all TB parameters, using  $\eta = 5 \text{ meV}$  and  $T=0 \text{ K}$ , are reported in Table I. As we can see, the inclusion of the higher-order terms is crucial to give rise to a finite infrared activity.

In order to investigate the role of each TB parameter on the infrared activity, we consider a set of toy TB model, based on our present parameter set where, keeping the terms  $\gamma_0$  and  $\gamma_1$  fixed, we “switch on”, one by one, the remaining TB parameters  $\gamma_2, \gamma_3, \gamma_4, \gamma_5$  and the crystal field  $\Delta$ . The chemical potential is evaluated self-consistently in each model to preserve the charge neutrality. The results are summarized in Table I, where one can clearly see how the onset of infrared activity is directly related to the breaking of the particle-hole symmetry. Within this scenario, the detailed optical properties result from a complex balance between all TB parameters.

To estimate the sensitivity of the predictions of the

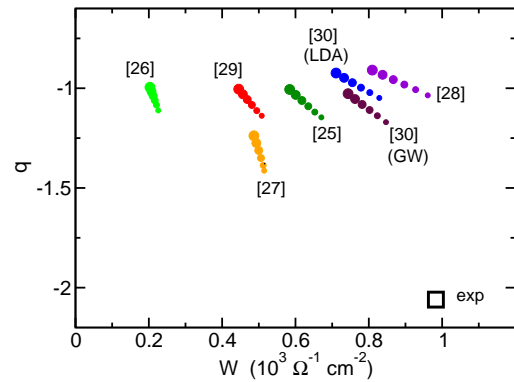


FIG. 4: Phase diagram of the phonon strength  $W$  vs. the Fano parameter  $q$ . The empty square represents our experimental values, filled circles represent data obtained at  $T = 10 \text{ K}$  by using different TB models available in literature.<sup>25-30</sup> The size of symbols for the theoretical data is proportional to the damping term  $\eta = 5, \dots, 30 \text{ meV}$ .

charged-phonon model on the particular choice of the TB model, we calculated the phonon strength  $W$  and the Fano factor  $q$  obtained from different TB parameter sets proposed in literature for graphite.<sup>25–30</sup> The results are summarized in Fig. 4, where we also show the experimental values of  $W$  and  $q$  at 10 K. The large spread of the theoretical points in the  $W$ - $q$  diagram reveals that relatively small changes in the underlying electronic structure affect significantly the phonon properties. Given the high sensitivity of the results of the charged-phonon model on the electronic details and some uncertainty related to the choice of the momentum cutoff  $\bar{k}$ , the comparison with the experimental finding seems to be reasonably good. Importantly, the model predicts correctly the large value of the experimental spectral intensity  $W$  and therefore the effective infrared charge. This is a significant improvement as compared to a previous calculation based on a generalized bond-charge model,<sup>16</sup> which predicts the effective charge of this mode to be an order of magnitude smaller. The charge-phonon theory also accounts for (and even overestimates) the strong Fano lineshape asymmetry. It should be noted, however, that the precise value of the Fano parameter  $q$  is also quite sensitive to the damping magnitude, which is sample dependent and should be regarded as an adjustable parameter in the present model.

It is interesting to compare the temperature dependence of the phonon parameters shown in Fig. 2 with the theoretical calculations (dashed lines). The frequency shift and the linewidth of the phonon peak here are evaluated via the phonon self energy  $\Pi(\omega)$ :  $\Delta\omega_0 = \hbar^{-1}\text{Re}[\Pi(\omega_0)]$ ,  $\Gamma = -\hbar^{-1}\text{Im}[\Pi(\omega_0)]$ , while the spectral weight and the asymmetry parameter are obtained using the given above formulas. We can notice that for all

parameters the theory strongly underestimates the temperature variation as compared to the experiment. We believe that the strong temperature dependence of the experimental features is a signature of anharmonic effects induced by the phonon-phonon scattering. A careful study of such anharmonic effects within the density functional theory context was provided in Ref. 3, where these effects were found to be mostly responsible for the thermal variation of the phonon frequency and the linewidth. It is likely that the phonon anharmonicity is also responsible for a sizeable temperature dependence of the spectral weight and the Fano asymmetry. The theoretical treatment of anharmonicity within the charged-phonon theory is an interesting problem which is beyond the scope of the present work.

In conclusion, we have investigated the origin of the infrared phonon activity of the  $E_u$  mode at  $\omega \approx 1590 \text{ cm}^{-1}$  in pristine graphite. We experimentally found that the effective infrared charge is close to 0.3 electrons, which is an exceptionally large value for an elemental compound. A significant Fano asymmetry is also present ( $q \approx -2$ ). We have shown that both these observations can be explained within the framework of the charged-phonon theory, where a crucial role is played by the broken particle-hole symmetry associated with the higher-order tight-binding terms. The approach used in this work can be extended to other related materials, such as carbon nanotubes and intercalated graphite.

We thank Lara Benfatto for many useful discussions. E.C. acknowledges the Marie Curie grant PIEF-GA-2009-251904. The work of A.B.K. was supported by the grant No.200020-130093 of the Swiss National Science Foundation (SNSF).

- 
- <sup>1</sup> S. Pisana, M. Lazzeri, C. Casiraghi, K.S. Novoselov, A.K. Geim, A.C. Ferrari, and F. Mauri, *Nat. Mater.* **6**, 198 (2007).
  - <sup>2</sup> J. Yan, Y. Zhang, P. Kim, and A. Pinczuk, *Phys. Rev. Lett.* **98**, 166802 (2007).
  - <sup>3</sup> N. Bonini, M. Lazzeri, N. Marzari, and F. Mauri, *Phys. Rev. Lett.* **99**, 176802 (2007).
  - <sup>4</sup> L.M. Malard, D.C. Elias, E.S. Alves, and M.A. Pimenta, *Phys. Rev. Lett.* **101**, 257401 (2008).
  - <sup>5</sup> J. Yan, T. Villarsen, E.A. Henriksen, P. Kim, and A. Pinczuk, *Phys. Rev. B* **80**, 241417(R) (2009).
  - <sup>6</sup> P. Gava, M. Lazzeri, A.M. Saitta, and F. Mauri, *Phys. Rev. B* **80**, 155422 (2009).
  - <sup>7</sup> D.L. Mafra, L.M. Malard, S.K. Doorn, H. Htoon, J. Nilsson, A.H. Castro Neto, and M.A. Pimenta, *Phys. Rev. B* **80**, 241414 (2009).
  - <sup>8</sup> A.B. Kuzmenko, L. Benfatto, E. Cappelluti, I. Crassee, D. van der Marel, P. Blake, K.S. Novoselov, and A. K. Geim, *Phys. Rev. Lett.* **103**, 116804 (2009).
  - <sup>9</sup> T.-Ta Tang *et al.*, *Nat. Nanotechn.* **5**, 32 (2010).
  - <sup>10</sup> Z.Q. Li, C.H. Lui, E. Cappelluti, L. Benfatto, K.F. Mak, G.L. Carr, J. Shen, and T.F. Heinz, *Phys. Rev. Lett.* **108**, 156801 (2012).
  - <sup>11</sup> Z. Liu, X. Lu, P. Peng, W. Wu, S.-S. Pei, Q. Yu, and J. Bao, *Phys. Rev. B* **82**, 155435 (2010).
  - <sup>12</sup> R.J. Nemanich, G. Lucovsky, and S.A. Solin, *Solid State Comm.* **23**, 117 (1977).
  - <sup>13</sup> C. Underhill, S.Y. Leung, G. Dresselhaus, and M.S. Dresselhaus, *Solid State Comm.* **29**, 769 (1979).
  - <sup>14</sup> S. Tongay, J. Hwang, D.B. Tanner, H.K. Pal, D. Maslov, and A.F. Hebard, *Phys. Rev. B* **81**, 115428 (2010).
  - <sup>15</sup> J. Humlíček, A. Nebojsa, F. Munz, M. Miric, and R. Gajic, *Thin Solid Films* **519**, 2624 (2011).
  - <sup>16</sup> G.S. Jeon and G.D. Mahan, *Phys. Rev. B* **71**, 184306 (2005).
  - <sup>17</sup> E. Cappelluti, L. Benfatto, and A.B. Kuzmenko, *Phys. Rev. B* **82**, 041402 (2010).
  - <sup>18</sup> A.B. Kuzmenko, E. van Heumen, F. Carbone, and D. van der Marel, *Phys. Rev. Lett.* **100**, 117401 (2008).
  - <sup>19</sup> U. Fano, *Phys. Rev.* **124**, 1866 (1961).
  - <sup>20</sup> M.J. Rice and H.Y. Choi, *Phys. Rev. B* **45**, 10173 (1992).
  - <sup>21</sup> T. Ando, *J. Phys. Soc. Japan* **76**, 104711 (2007).
  - <sup>22</sup> S. Piscanec, M. Lazzeri, F. Mauri, A.C. Ferrari, and J. Robertson, *Phys. Rev. Lett.* **93**, 185503 (2004).

- <sup>23</sup> M. Lazzeri, C. Attacalite, L. Wirtz, and F. Mauri, Phys. Rev. B **78**, 081406 (2008).
- <sup>24</sup> E. Cappelluti and G. Profeta. arXiv:1202.5786, Phys. Rev. B (in print).
- <sup>25</sup> J. Levallois, M.K. Tran, and A. B. Kuzmenko. Solid State Communication, in press; DOI: 10.1016/j.ssc.2012.04.036.
- <sup>26</sup> M. S. Dresselhaus e G. Dresselhaus, Advanced in Physics **51**, 1 (2002)
- <sup>27</sup> R.C. Tatar and S. Rabi, Phys. Rev. B **25**, 4126 (1982).
- <sup>28</sup> J.C. Charlier, X. Gonze, and J.P. Michenaud, Phys. Rev. B **43**, (1991).
- <sup>29</sup> B. Partoens and F.M. Peeters, Phys. Rev. B **74**, 075404 (2006).
- <sup>30</sup> A. Gruneis, C. Attacalite, L. Wirtz, H. Shiozawa, R. Saito, T. Pichler, and A. Rubio, Phys. Rev. B **78**, 205425 (2008).